Workshop on Virtual Reality Interaction and Physical Simulation VRIPHYS (2012)
J. Bender, A. Kuijper, D. W. Fellner, and É. Guérin (Editors)

Efficient Breast Deformation Simulation

M. T. Harz[†1], J. Georgii[1], L. Wang[1], K. Schilling[2], and H.-O. Peitgen[1]

[1]Fraunhofer MEVIS, Bremen, Germany
[2]Boca Raton Regional Hospital, Boca Raton (FL), U.S.A.

Abstract

Breast surgery might benefit from image guidance, if position and extend of the disease could be visualized in the same breast deformation as the surgery is performed. Such visualizations, however, are challenging to obtain, since the positioning for image acquisition in MRI is prone, while the patient lies supine for surgical procedures, causing a considerable deformation of the breasts between the two states. In our contribution, we outline a set of novel algorithms and methods to improve an efficient simulation of breast deformation between the prone image and the supine surgery positioning. In particular, we propose several extensions to a highly efficient dynamic corotated finite element method (FEM), namely non-linear material properties, the sliding of the breast tissue on the chest wall, and a fine-tuning step to align the breast model to a measured surface. All extensions are carefully designed to keep the efficiency and stability of the approach, and thus to allow their application in clinical routine. We explore all novel techniques using synthetic and volunteer prone and supine breast MRI data and assess their feasibility towards accurate, yet efficient simulation of large breast deformations.

Categories and Subject Descriptors (according to ACM CCS): I.3.5 [Computational Geometry and Object Modeling]: Physically based modeling—Curve, surface, solid, and object representations

1. Introduction

Breast cancers that are detected early and – for example by biopsy and MRI imaging – determined to be locally invasive only, are eligible for breast conserving therapy, where only the cancerous tissue together with a safety margin is excavated. These therapy approaches, however, suffer recurrence rates from 8% to 14%, and specimen pathology reveals positive (cancerous) margins in between 17% to 59% of the cases [CSH*11]. Additionally, although the procedure is comparatively easy and routine, poor cosmetic outcomes are frequent complications, which is due to the way of indicating the target area with metal wire guides that are inserted under mammographic or MR image guidance, and that serve as a surgery path indicator to the surgeon. In effect, depending on lesion position and wire insertion direction, this can cause suboptimal access paths leading through unnecessary long parts of healthy tissue instead of shortest paths from skin incision to lesion. Additionally, the required safety margins in this setup are large, and still not always met when the diseased area is invisible intraoperatively.

Several attempts have been made to improve surgical outcomes, e.g. incorporating intra-operative ultrasound imaging. Some authors propose robot aid for the placement of biopsy needles [MSP10], but require a fixated breast where the needle is placed. Approaches that help the surgeon to navigate more safely are more challenging and less developed. The study of [ALP*10] uses MRI-based navigation and tackles the problem of tracking the breast surface from a supine MRI scan to the surgery position, but neither support navigation in open breast surgery nor account for the much more challenging deformations from the prone positioning. Support of open surgery is attempted in the ultrasonography-based approach presented by [SNT*98]. Their approach, however, requires a tracking equipment to be positioned in the operating room, and will display the superimposed target area only in a computer monitor.

Another approach is to simulate the deformation of the breast from the known shape seen in the diagnostic MRI scans (in prone positioning, meaning face-down) into the shape seen in the face-up, supine, positioning on the surgery table. This approach is commonly known as the prone-to-supine deformation and has been tackled in several publications. To understand the difficulty to simulate this defor-

† markus.harz@mevis.fraunhofer.de

DOI: 10.2312/PE/vriphys/vriphys12/117-126

Figure 1: *Breast anatomy. Fatty tissue (orange in the picture) encloses the parenchymal structures, consisting of the terminal ductal lobular units (TDLUs, brown-purple), from where the ducts extend to the nipple. To the left, the rib cage with the pectoral muscle delimits the breast tissues. Image courtesy of Patrick J. Lynch and C. Carl Jaffe; Creative Commons Attribution 2.5 Generic license.*

mation, a brief account of the biological composition and biomechanical behavior of breast tissues is required (see also Fig. 1). The breast shape is predominantly governed by four tissue types: (1) the skin, which is nearly incompressible but capable of virtually unconstrained shear movements; (2) the fatty tissue, which can be conceptualized as small lumps that are not interconnected and hence behave like a viscous fluid; (3) the glandular tissue, namely milk ducts and lobules, which are connected to the nipple and partially to the fatty/stromal tissue surrounding them, and are not extensible; and (4) the Cooper ligaments, a connective tissue reaching from the subcutaneous tissues to the chest wall and accounting for the breast shape for the most part. They are not connected to any other tissue. In MRI, the fatty and glandular tissues can be seen and segmented, sometimes also the skin layer can be estimated. Cooper ligaments are not visible due to the limited image resolution.

Concerning breast tissue modeling, these tissue types and their interconnectedness can hardly be accounted for in a realistic manner. Building a model on a fine enough scale to depict all relevant tissue types will lead to infeasible computational effort, such that the more promising option is a modeling at a coarser scale. Of these, different variants exist, out of which some attempt to model heterogeneous tissue types, others assume homogenous material, but introduce anisotropy and non-linear material laws (cf. [TWG*11, WGCB07] for comparisons of selected approaches).

Pertaining to the task of prone-to-supine deformation simulation, researchers have tried to match the breast shapes or to derive one from the other by employing finite element analysis using non-linear material laws [RCB*07, RNHN08]. However, the patient-specific modeling effort and computational complexity of this approach are both high and thus unlikely to be employed in clinical routine. The fastest available implementations of dynamic non-linear models [HHM*11] are based on explicit finite element approaches, which limit the magnitude of the largest possible time step in a dynamic simulation by the well-known Courant condition. Meanwhile, other research has looked at the feasibility of pseudo non-linear finite elasticity simulations and found them to be close, though not equal, to fully non-linear finite elasticity formulations [WGCB07]. These pseudo non-linear formulations are closest to the work we propose in this contribution.

Other work focuses on augmented reality approaches, displaying target structures on the skin of the patient, after calculating the transformation from prone to supine. While this is not sufficient for our purposes, the contributions of [CTC*06] and [dPCH*08] address many aspects that we are dealing with as well. Still, to the best of our knowledge a setup as ours has not been proposed before.

1.1. Contribution

We use prone MRI scans to automatically create a patient-specific model of the breast to model the deformation from the prone position (using breast coils) to the supine position used for surgical procedures. We extend an approach that combines automatic segmentation with the generation of multi-resolution hexahedral meshes [HGSH11], which are an effective basis for fast, efficient deformation simulations [DGBW08, DGW11].

Our goal is to improve the modeling of breast deformations incorporating isotropic non-linear material laws [HGSH11]. In this work, the authors propose an per-element elastic modulus update in every simulation step to mimic a non-linear material law. The rationale to assume homogeneous tissue in the first place, is that – as described above – for a realistic simulation the required level of detail is beyond computational feasibility for our application. Instead we will enhance the efficient deformation simulation approach with algorithms that improve the plausibility and accuracy of the results while keeping the computational efficiency of the approach. Therefore, the approach is suitable for extensions towards intra-surgery deformation tracking, which is one of the goals of our work.

We introduce (1) a time step reversal mechanism that ef-

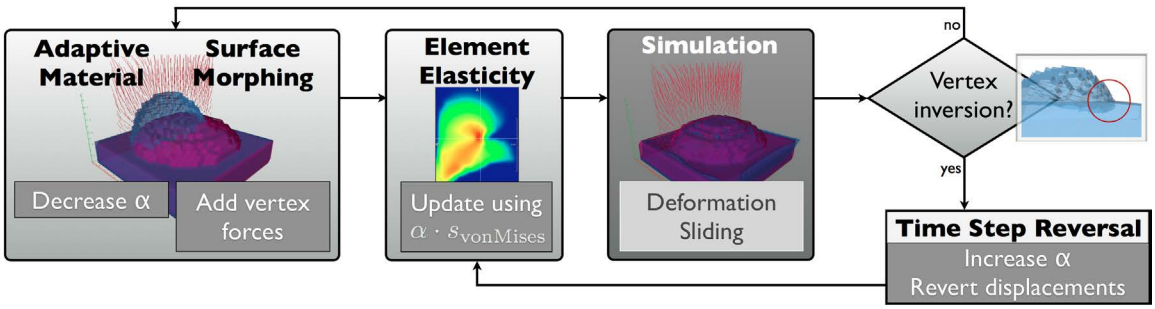

Figure 2: *Outline of the simulation steps arranged in a feedback loop. The loop allows for undo operations of those simulation steps that result in inverted elements.*

fectively avoids inverted elements when adjusting the per-element elastic modulus in a simulation step, (2) the simulation of sliding between interfacing bodies governed by vertex forces under friction, and lastly (3) a method to deform a body towards a target surface.

First, we use the element stress to systematically adjust the per-element elastic modulus between single time steps of the simulation, which effectively models an isotropic non-linear material law. We extend existing work by a time step reversal mechanism such that unconditional stability under dynamic simulation is maintained (Section 2.3).

Second, we strive to model biologically observed behaviors of breast tissue that is not rigidly fixated to the chest wall, but has the freedom to slide on the chest wall. In the works presented here, we have accounted for this by a novel method that calculates the sliding of the breast tissue on the chest wall proportional to the forces induced by the simulation, e.g. caused by gravity (Section 2.4).

Third, we propose a mechanism that applies forces to surface vertices of the deformable body such that a known target shape is approximated closely. We use a distance transformation of the target surface to efficiently compute the forces required for the morphing. We apply this addition to the results of a prior deformation simulation that approximates the desired target deformation with only small remaining local errors (Section 2.5).

Our overall method maintains its computationally beneficial properties: It avoids complicated measurements to determine non-linear material parameters, and it can be integrated into existing corotated linear-elastic code. We approximate microscopic material tissue properties on a macroscopic scale by modifying the material under load to emulate natural behavior. Inverted finite elements are avoided by the time step reversal mechanism presented.

All algorithms described before are modular additions to the basic simulation code. They can be parameterized and arbitrarily enabled and disabled. We hence propose a combined pipeline according to Figure 2. The processing iteratively performs the following steps:

1. Add vertex forces at current displaced positions (Surface morphing).
2. Update element elasticity based on von Mises stress and α.
3. Simulate: calculate new displacement field.
4. Check for inverted elements
   a. If none, decrease α; back to 1.
   b. If inverted elements, increase α and revert positions; back to 2.

2. Material and Methods

Our proposed system starts with MR images taken in the prone position that are automatically segmented into deformable and fixed tissues using the methods proposed by [WFFH11]. These methods have been adjusted to provide necessary information for the sliding approach, as it will be described in more detail in this section. The segmentation is used to setup the FE model. A highly efficient FEM-based breast deformation approach is then used to simulate the shape change from prone MRI to the desired patient position, even allowing for real-time simulations of breast/patient repositioning at moderate mesh resolutions, which is relevant for the surgery scenario depicted above. An overview of the interplay of the single algorithmic steps is given in Figure 2.

2.1. Model Generation

Our overall approach is designed to work in clinical practice; hence we have devised tools to support automatic patient-specific model generation from image acquisition to initialization of simulation, including the segmentation into the relevant tissues. This goes beyond other work, where the meshing is automatic, but requires undisclosed efforts for segmentation [RSM*06]. The algorithmic methods described in the following sections are novel developments that

have been applied to volunteer data. For a thorough analysis, we additionally describe results based on computational phantoms that exhibit characteristics suitable to demonstrate the benefits of the proposed methods, and sketch the benefits on volunteer data by example.

The software phantom used for most developments is a half-ellipsoidal shape that is modified to resemble prone and supine shapes of the breast. These shapes are easy to generate in any size and resolution.

2.2. Breast Deformation Simulation

Our approach is based on a multigrid finite element framework [GW08], which efficiently simulates deformations of the breasts using the so-called co-rotated Cauchy strain formulation [RB86]. One novel aspect of our work is to update the per-element elastic modulus based on the shape change that the element experiences in a given simulation step. By this explicit per-element elasticity update, we effectively model a non-linear isotropic material law.

The deformation of a volumetric object is described by a displacement field $u(x)$, $u : \mathbb{R}^3 \to \mathbb{R}^3$; $x \in \mathbb{R}^3$, which maps the reference configuration Ω to the deformed configuration $\{x + u(x) \mid x \in \Omega\}$. Driven by external forces f, a deformed solid is governed by the well-known Lagrangian equation of motion, $M\ddot{u} + C\dot{u} + Ku = f$, where M, C, and K are respectively known as the mass, damping and stiffness matrices, u denotes the composition of the displacement vectors of all vertices, and f consists of the force vectors applied to these vertices. The stiffness matrix K is assembled from the so-called element stiffness matrices K^e. Typically, every element in a finite element discretization has only a very small number of neighbors, and thus the resulting stiffness matrix is very sparse. The element matrices are precomputed with a fixed elastic modulus E_0. Due to the linearity of the underlying material law, the element matrix of a particular element can then be obtained by scaling K^e by the stiffness value of this element relative to $E_0 \in \mathbb{R}$. Therefore, we can update the stiffness values within the assembling process of the corotational formulation at nearly no additional computational costs and thus achieve a fast update of stiffness values in the FE model analogously to previous approaches [DGBW08, SGW07]. To efficiently update the data structures of the numerical multigrid solver, we make use of a fast approach to compute sparse-sparse matrix products [GW10].

2.3. Improved Non-linear Material Modeling Using Time Step Reversal

Our approach to model non-linear material behavior is motivated by the observation that in a model coarse enough for real-time update speeds, a very low Elastic modulus is required to account for the dominant contribution of fatty (loosely coupled) tissue in breast deformations. However, this yields unrealistic behavior for large deformations, manifested in inverted elements at contact points or in folds. Locally stiffening the material at these points effectively prevents this behavior [HGSH11].

To model the non-linear material law aspect responsible for a macroscopic stiffening of material under stress, in our contribution we use the von-Mises stress tensor norm [Bat02] to quantify the element stress,

$$\sigma_{\text{Mises}} = \sqrt{3 \sum_{k=4}^{6} \sigma_k^2 + \frac{3}{2} \sum_{k=1}^{3} (\sigma_k - \bar{\sigma})^2} \,. \tag{1}$$

The von-Mises norm provides a rotation-invariant scalar metric of the overall stress imposed on an element. We assume that breast tissue is composed of lumps of material that can move about with little friction. Macroscopically, this requires a small elastic modulus to observe realistic deformations. However, under compression real-world material exhibits a non-linear behavior, since now the stiff tissue parts determine the material behavior rather than the low-friction movements, i.e., macroscopically the stiffness increases with the stress.

The element relative elastic modulus can be modified per simulated time step according to $E_r = 1 + \alpha \cdot s_{\text{VM}}$ with $\alpha \in \mathbb{R}$ a user-defined scalar factor greater than zero and $s_{\text{VM}} \in \mathbb{R}$ the von Mises stress norm.

These explicit updates of the per-element elastic modulus have to be performed carefully to ensure stability of the approach, because internal forces in the body are mainly proportional to the elastic modulus, and thus updating this value while the deformation is not modified increases the stored elastic energy. Instead of limiting the elasticity update by damping [HGSH11], we propose a novel mechanism that adapts the α such that instabilities are avoided at all. Since α is no longer fixed, two things are required: (1) a mechanism to try out a guess for α, and (2) a metric for the goodness of α. Our metric is a binary decision on the integrity of the mesh, indicated by the lack of inverted finite elements. Inverted elements occur when the time step is too big given the current forces imposed on the vertices. Then, physically implausible vertex positions are the only numerically valid solution to the FEM system of equations. Consequently, our approach to avoid inverted elements is to revert a simulation time step, increase α, and repeat the time step. This can be done iteratively until the first suitable α is found that stiffens the elements enough to withstand the forces in the simulation time step without inversion.

The time step reversal is of course only possible with a time integration scheme that allows for a storage of all characteristic information of the mesh in each time step, such that it can be reverted. This is for example the case for dynamic Euler integration where all information is contained in any two consecutive displacement fields. Consequently, it is sufficient to store u_{t_0-1} and u_{t_0} to revert to the simulation

state at time t_0. Our actual implementation even allows for an "undo" history, by using n time step reversal plugins that store a simulation state in a round-robin fashion. Then, the simulation can be reverted to any of the n stored states, and continued from there.

Once the simulation proceeds, α can be decreased again to enable a maximum movement of the breast tissue. Note that some careful control has to be added to avoid consecutively increase and decrease of α. However, our implementation does not dependent on user-provided parameters. Instead, from an initial α set by the user, the simulation starts, and only when an inverted element is detected, α is adjusted as described above. Now, when relaxation of α starts, we detect oscillations: as soon as α has been decreased, increased, and decreased again, we adjust the speed of α changes proportional to the magnitude of α. This eventually converges to a stable α. For performance reasons, α should initially be set to a knowingly too high value, and the algorithm will decrease it as described.

Note, however, that a new α has to be found if any of the boundary conditions change, in particular, if the direction of gravity changes, which is relevant in our scenario. In our application the deformation simulation does not require to run at a constant update rate, and especially the computationally challenging deformation from prone to supine can be performed before the intervention.

2.4. Emulating Breast Tissue Sliding on Chest Wall

While in previous work Dirichlet boundary conditions were applied on the vertices on the breast-chest interface, we herein propose to replace the fixations by displacement constraints that are updated in each simulation time step similar to the approach of [GLDW10]. This enables us to emulate a sliding of the tissue on the chest wall, governed by friction, with the possibility to include inertia effects.

This is implemented by computing the forces for all vertices that have a displacement constraint, and projecting the resulting force vector into the plane locally tangential to the chest wall. To find this tangential plane, prior to the simulation a vector field is calculated from the chest wall mask obtained in the segmentation step, by running a 3D derivative of Gaussian filter with a $\sigma = 2\,\text{mm}$ over the image to obtain a vector field that is guaranteed to be dense around the vertices. 2 mm are chosen because this is roughly twice the in-plane voxel resolution of current morphological MRI sequences, such that a mild averaging is obtained.

For the application of sliding in the breast, it can be observed from prone-supine control scans, that not all breast tissue will slide equally freely. For example, with both breasts moving around the chest wall to opposed sides of the chest in supine positioning, the medial tissue will be restricted in movement by the skin. In general, our hypothesis is that the amount of sliding is proportional to the local thickness of the tissue, or, the perpendicular distance from the chest wall to the skin in a hypothetic gravity-free state. Thus, limiting factors are implemented to tune the sliding to match the empirically observed behaviour. Of course, this calculation can also be bypassed to allow arbitrary sliding governed by friction and shape alone. Out of different limiting factors, a Gaussian shaping of the permissible shift may be used to model the observation that the breast will not slide near the sternum, nor near the axilla. This is controlled by a bimodal 2-dimensional Gaussian function

$$z = Ae^{-\left(\frac{(x-x_0)^2}{2\cdot\sigma_x\cdot\sigma_x}+\frac{(y-y_0)^2}{2\cdot\sigma_y\cdot\sigma_y}\right)} + Ae^{-\left(\frac{(x-x_1)^2}{2\cdot\sigma_x\cdot\sigma_x}+\frac{(y-y_0)^2}{2\cdot\sigma_y\cdot\sigma_y}\right)},$$

and calculating the sliding displacement d as $d = d + zD_f$. The two modes are preferably centered at the breast centers in the xz-plane, and should have σ set such that the extend of the breasts is covered. To this end, the center of the breasts can be determined automatically based on the nipple positions known from our segmentation algorithm, while an appropriate value for σ is obtained by simply setting it to half of the diameter of one breast which again is roughly one quarter of the image's bounding box.

It is particularly noteworthy that this implementation does not require an analytical model of the surface to be known, but works with any given geometry. Also, it is physiologically motivated, whereas movement on approximated analytical surfaces like in [MHH*12] is not.

2.5. Surface Morphing Using a Distance Field

If the target surface is known, for example by a surface scan acquired during the intervention, or if any other information is known about where displaced landmarks have moved, we propose to morph the model to the target surface by applying forces at specific vertices of the finite element mesh. By means of this approach we can achieve a better matching of the model and the patient if we assume the surfaces to be sufficiently close in the beginning. However, as a side note let us mention that this step is not amenable to capture the whole prone-supine deformation in the interior. This being said, for a known target surface, we propose the following approach.

Firstly, we represent the target surface in a three-dimensional image, from which we calculate the three-dimensional Euclidean distance transformation. On this, we apply a likewise three-dimensional derivative of Gaussians kernel filter, such that a dense vector field is obtained, where at each point the vector points into the direction of the shortest path to the target surface. This vector field is then scaled with the Euclidean distance to obtain larger forces far from the target surface and smaller force updates close to it. In all, calculation of the distance field is done in 2-4 sec depending on image size, and can easily be sped up using GPU implementations of distance transform [SKW10] and Gauss filtering to be feasible for interactive updates of the surface morphing.

Given the finite element mesh we determine the distance vector at the position of the displaced surface vertices. A force proportional to the vector's length (which is again proportional to the distance from the target surface) is applied in direction of the vector. Note that forces are accumulative: after every simulation step, the force is read at the new image position, and added to the force already stored at the vertex. Note that due to the dynamics of the simulation overshooting of the displacements might occur; however, since the vectors added in the next step in these cases resemble a force into the opposite direction the approach still converges as expected. Note, that our implementation might be used to affect only subsets of the vertices, e.g. only surface vertices, or only those that have no other constraints (fixation, displacement, etc.).

2.6. Combined Pipeline

With the combination of the above methods according to 2, we aim to improve the overall quantifiable accuracy of deformation obtained. Regarding the figure, a noteworthy property is that the vertex forces accumulated for a node never need to be reset explicitly: In case inverted elements are detected in step 4., no forces at the current positions are added, because the algorithm continues with an update of elasticity (step 2), skipping vertex force estimation. The vertex positions, however, are restored to the state before the current. Consequently, the vertices are again in the positions where they received the last vertex force update (which has not been reset), but elements will be stiffer now due to the increased α. The next iteration starts at step 2., with forces like in the previous iteration. With a target surface given, the decrease of α will be stopped when a sufficiently "soft" material to achieve the required deformation is achieved, based on a computation of surface distances from the distance field.

It is important to know the limitations of each individual method, and their interdependence and objective for application. Particularly for the surface morphing algorithm, we do not propose to use it before the physically more realistic sliding- and stiffness update-based computations have been computed until macroscopic stability.

We have so far successfully applied the proposed pipeline of algorithms to the breast model situation depicted in 5 and can state that generally the combination of the algorithms increases the robustness and quality of the overall approach.

3. Results and Discussion

Aiming at support for breast surgery planning and intervention support, a quantitative evaluation of accuracy is the most obvious requirement to translate algorithmic developments into clinically applicable solutions. Currently, we lack data for this level of evaluation, and acknowledge that based on visual inspection, algorithmic improvements should first be implemented. Still, motivated by the promising results so far, we firstly prove the clinical applicability in terms of speed requirement.

An important goal is to maintain the performance of the underlying corotatonal finite element framework, so that interactive adjustments are possible, for example to manipulate the orientation of the gravity vector to match simulation and observed patient positioning on the surgery/biopsy table. Therefore, we have evaluated the performance on several data sets with 50k to 300k elements, and observed the expected linear scaling of execution time with the number of mesh elements for one time step. Table 3 lists timings for the simulation including the elastic modulus update and the sliding on the chest wall.

The timings in Table 3 were measured on an Intel Core i7 Quad 2.66GHz CPU. Note that the timings are dominated by the time required by the simulation step. The additional time required to update the elastic modulus of each element and to compute the sliding on the chest wall is small as can be seen in the respective column (up./sl.). The time step reversal increases the number of total simulation steps and is therefore not reflected in the table. We remark that the simulations are not necessarily converged after 25 iterations, though in our experience the deformations imposed by gravity are typically settling after 0.5 to 1.0 sec wall time, i.e. after 15-30 iterations with time steps of 0.033 sec.

In the following, we independently assess the benefits contributed by the three proposed extensions.

3.1. Elasticity Update with Time Step Reversal

Of the questions to ask regarding the deformation of tissue under simulated force, one is how the material parameters influence the results. In our context we were interested how sensitive the stiffness update calculation to changes in elastic modulus and compressibility. Elasticity updates also introduce non-linearities that can potentially result in oscillations, and in particular in combination with the time step reversal approach, it is crucial to establish the stability and robustness of the approach.

We have hence used computational phantoms prior to the application to breast MRI data. In these experiments, the proposed update criterion was able to produce stable large deformations of the model in a robust fashion, in particular without changing any of the simulation parameters.

For the patient data based evaluation, a Poisson ratio of 0.48 and a base elastic modulus of $2 \cdot 10^3$ Pa were chosen based on literature values to characterise the breast tissue material [HHM*11]. In our experiments, the fraction of time reversal steps was about 20% of all simulation steps until convergence to a stable state. This can be assumed to be a worst case scenario: α was initially chosen one order of magnitude too high and the α decrease factor (and consequently also the increase factor for reverted time steps) was set to a

Table 1: *Timing statistics. 25 simulation time steps (sim.) were performed, and the same number of per-element elastic modulus update and sliding operations (up./sl.). Timings were measured on an Intel Core i7 Quad 2.66GHz CPU.*

#ele.	sim. [ms]	up./sl. [ms]	total 25 steps [sec]
47,895	189	35	5.6
99,390	400	73	11.8
158,340	644	109	18.8
158,340	628	109	18.4
313,335	1432	239	41.7

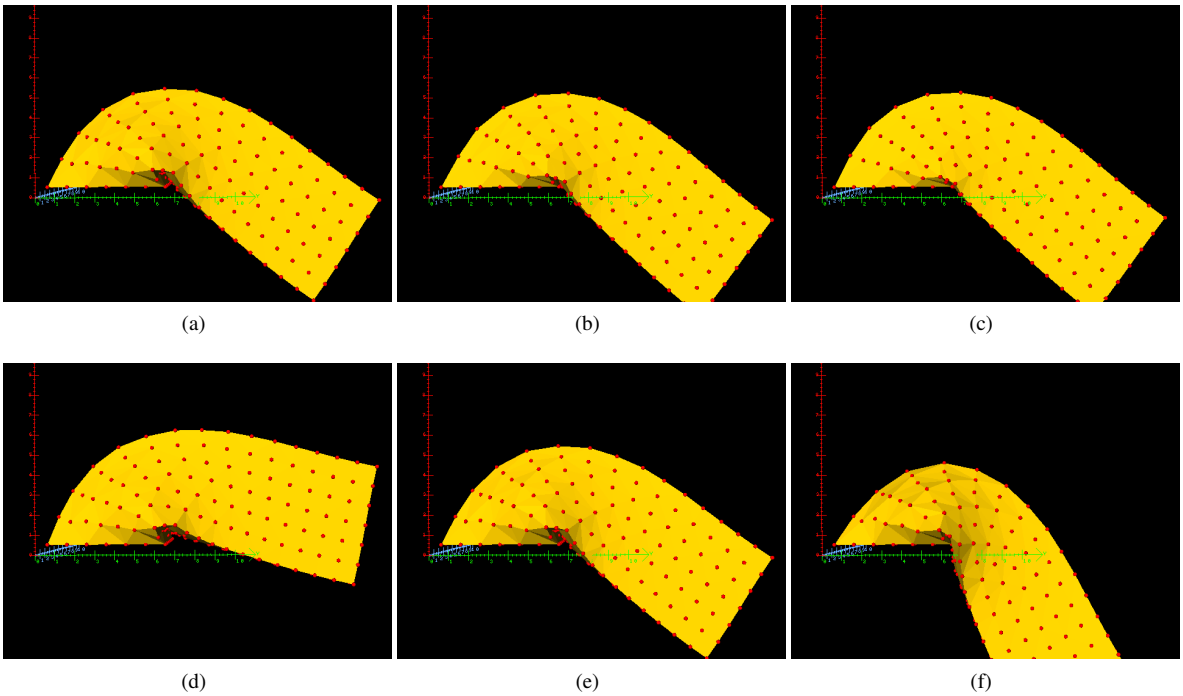

Figure 3: *Maximum deformation with* α *adapted for Poisson ratios of 0.48, 0.38, and 0.28 (a-c) and decreasing elastic moduli of 3000 kPa, 2000 kPa, and 1000 kPa (d-f).*

high value to arrive at a convergence fast. Under these conditions, the deformation simulation cannot keep pace with the elasticity drop caused by quickly decreasing α, such that inversion occurs several simulation steps "too late" and has to be reverted while α is increased again. Even under these advert conditions, our approach to find a suitable factor α by decreasing and increasing its value based on observed inverted elements has shown a robust behaviour. We have tested the method for different combinations of Poisson ratios and elastic modulus as shown in Figure 3. In practice, the parameters can be set to a robust general preset and the user will not have to adjust them. Again note, that a decrease of α to its limit is practically not necessarily required and has been conducted here to demonstrate the robustness near the limits of a given material's intrinsic capability to deform.

3.2. Sliding

Sliding has been examined on artificial and volunteer data. We have generated several computational phantoms ranging from simple proof-of-concept models to phantoms modelling two breasts on a curved chest wall to assess the behaviour of the sliding implementation in detail, before we .

In Figure 4, a dataset of a volunteer with a cup size of C to D has been asked to be imaged in prone and supine position. We have chosen this volunteer for presentation since larger breasts are obviously more difficult to model than small, stiffer breasts. Hence, we expected that the robustness and physical plausibility can be assessed more rigorously in this data. We have generated orthogonal cross-sections of both breasts after deformation simulation including the sliding al-

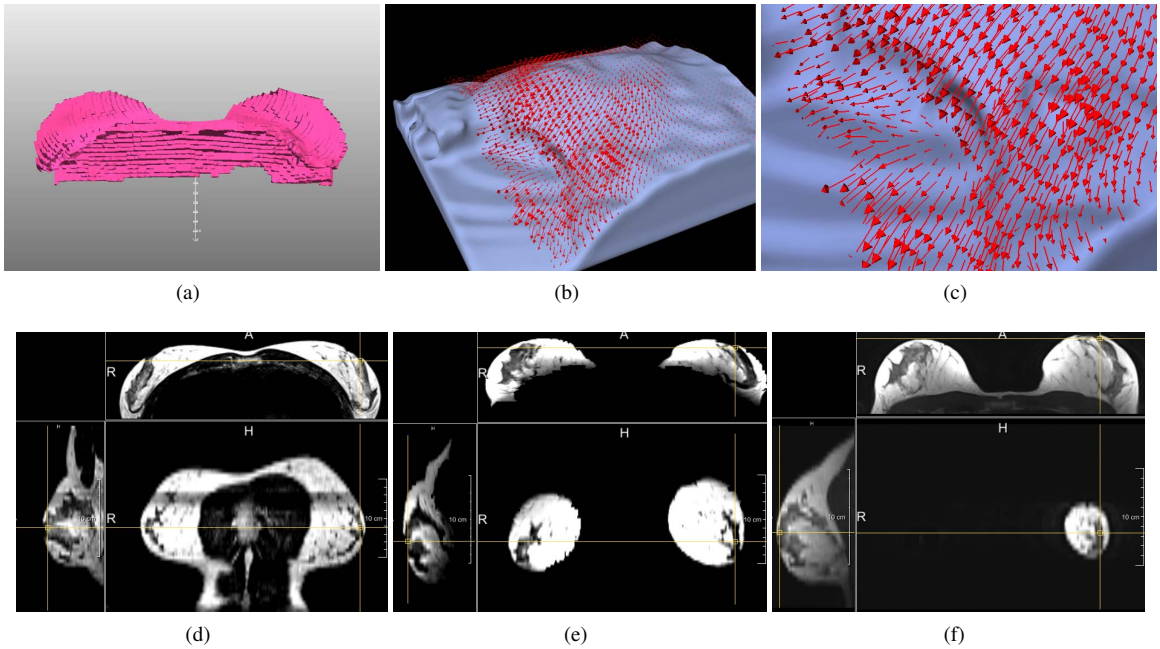

Figure 4: *Sliding simulation on volunteer data. (a) Surface rendering of the mesh after deformation simulation. (b,c) Vectors indicate the sliding. (d) Sections through the supine MRI, (e) through a corresponding location in the simulated supine MRI, and (f) for reference the undeformed, prone MRI.*

gorithm and – for this contribution – compared the result to the supine data at a matching cross section. Note how the slightly bent dark on bright structure in the transversal projection of the anatomically left breast (top cross section of the right breast in the prone image; Fig. 4(f)) is deformed in the simulated supine position (Fig. 4(e)). A current limitation to more realistic sliding results is that the arms are in the segmentation algorithm counted towards the chest wall, hence they support the breast tissue. This is seen in the magnification of the sliding vectors in Fig. 4(c).

3.3. Surface Morphing

Surface morphing has been developed using a breast software phantom consisting of a half ellipsoid that has been generated analytically in two configurations: one resembling the prone breast shape in the breast coil, and one resembling a stretched-out configuration in supine positioning. This is not the intended scenario for the application of the surface morphing algorithm, but rather a setup that is intended to display the performance under extreme conditions.

The configurations were constrained to have similar volumes and are both attached to a planar surface, so that the critical edge observed in MRI scans with breast coils is also modeled. To make the model as realistic as possible, we have moved the undeformed "prone" model out of the center of the "supine" model, and also applied gravity in a direction angulated out of orthogonality with respect to the plate. The back vertices of the planar surface have been fixated (Dirichlet boundary condition). The two structures can be seen in Figure 5(c), and consist of roughly 100k tetrahedral elements. Elasticity and Poisson ratio have been set to values similar to those used for the volunteer breast models described above.

Gravity has been simulated before the force field was applied to the surface vertices. But by means of our surface morphing, the target shape is closely approximated without any parameter adjustment, and in addition the final breast phantom volume is close to the volume of the target shape. Note in particular how the sharp edge between ground plate and breast model is adapted to the target shape.

On the volunteer data seen in Fig. 4, we have continued the simulation using surface morphing. Morphing in our volunteer dataset leads to about 30% volume loss of the model, because now the nodes attached to the chest wall are fixed rather than sliding, will forces press. Still, the surface morphing gives visibly better results than only using the sliding simulation. A current limitation to even higher deformations from surface morphing is that the chest wall model obtained from the prone data is bounded by the arms, hence the breasts cannot slide as much as in reality, and, as a consequence; we observe a loss of volume due to the surface

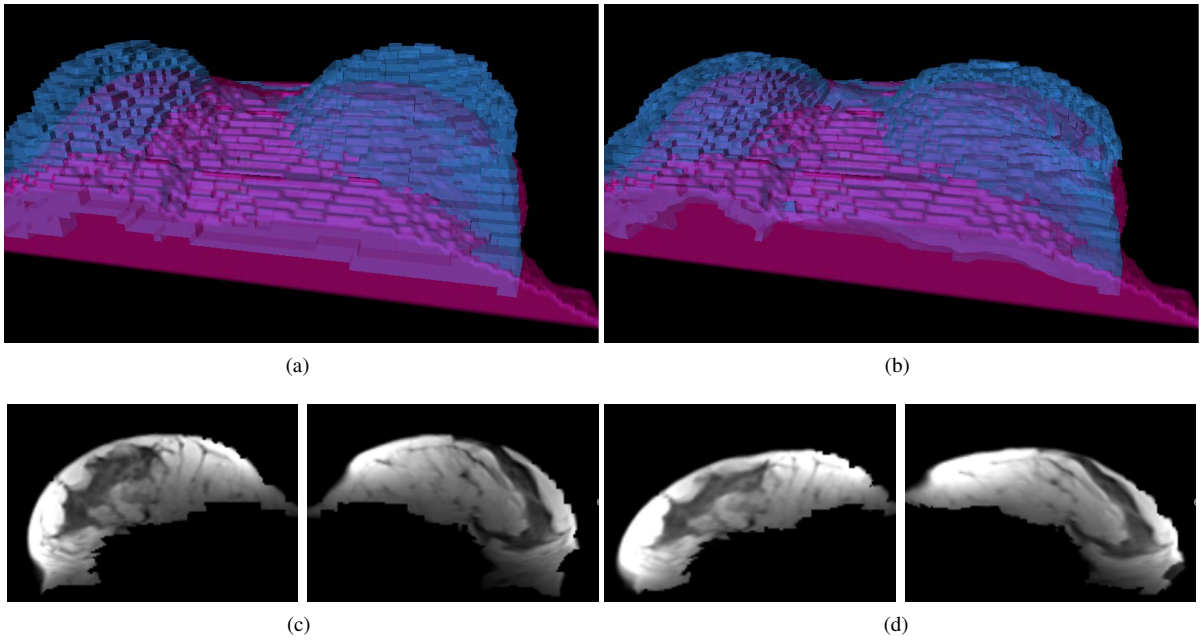

Figure 5: *Morphing the volunteer data. A volume mesh was generated from the result of a simulation using the sliding algorithm alone (cf. Fig. 4), and it was morphed to a target surface generated from the supine MRI data. (a) Model shape after sliding; (b) after surface morphing. (c),(d): Orthogonal reformatting of (a) and (b); same pos. as in Fig. 4.*

morphing step. We intend to solve this issue by improved determination of the chest wall model for sliding.

4. Conclusion

We have demonstrated a set of efficient algorithms that each individually improve simulation of breast deformations, and we have shown examples demonstrating the effectiveness of the approaches. By means of the automatic stiffness update in combination with the time step reversal, we are able to mimic the behaviour of breast tissue on a coarse scale, and thus we are able to achieve fast update rates of that approach.

The simulation of sliding boundary conditions on the chest wall is especially designed for the prone-supine deformation problem, where the breast tissue moves significantly along the chest wall; the benefit of our approach is that the sliding is determined automatically by inspecting the acting forces at the Dirichlet boundary conditions. Moreover, we have shown that a surface morphing approach can be successfully employed to deform one surface into the shape of a given second surface, even when they are not very similar.

We have proposed a pipeline joining all individual developments into a robust setup and demonstrated as a proof-of-concept the application of individual and combined algorithms to volunteer data, and of the pipeline to a breast phantom.

4.1. Future work

Our approach enables a number of future research directions which have the potential to further improve the specific clinical procedures. One idea is to extend the surface morphing approach by not only dragging the model to the target surface, but to adjust all boundary conditions (i.e. gravity direction) such that a situation with as little as possible local stress is obtained. We also intend to relax the mesh into a gravity-free state before simulation of gravity. In our work so far, we use a simple approach to determine the gravity-free state, which does not account for non-linearities in the material behaviour. We plan to refine the process of generating a gravity-free state similar to previous approaches, where the reference state was iteratively approximated from a loaded configuration [RCB*07]. In addition, for a realistic relaxation we want to estimate the unknown compression introduced by the breast coil during relaxation. All this is at the expense of additional computational costs.

We aim to derive robust parameters from patient-specific values such as breast volume and breast density, potentially also the structure of the parenchyma. This being accomplished, we aim to proceed to a formal, landmark-based quantitative evaluation of achievable precision based on volunteer data and compared our results with those of implementations using anisotropic non-linear material laws.

Also, our methods are not specific to the task of surgery

preparation or deformation tracking during surgery. They can equally well be employed to simulate the breast compression in other imaging procedures, like mammography or tomosynthesis, or whole breast ultrasound, or the matching of a pre-biopsy diagnostic MRI to the peri-interventional biopsy MRI where often the lesion position of interest is hard to recover. The versatility and easy configuration of all parts makes it also applicable to the simulation of organ deformation other than breasts for procedures that have currently insufficient support in the intervention setting, e.g. prostate deformation during transrectal biopsy.

Acknowledgements

This work was partially supported by the Fraunhofer Internal Programs under Grant No. MAVO 823 287 and by the German Federal Ministry of Education and Research (BMBF), project grant No. 01EX1012D.

References

[ALP*10] ALDERLIESTEN T., LOO C., PAAPE A., MULLER S., RUTGERS E., PEETERS M.-J. V., GILHUIJS K.: On the feasibility of MRI-guided navigation to demarcate breast cancer for breast-conserving surgery. *Medical physics 37*, 6 (2010), 2617–2626. 1

[Bat02] BATHE K.-J.: *Finite Element Procedures*. Prentice Hall, 2002. 4

[CSH*11] COOPEY S., SMITH B. L., HANSON S., BUCKLEY J., HUGHES K. S., GADD M., SPECHT M. C.: The Safety of Multiple Re-excisions after Lumpectomy for Breast Cancer. *Annals of surgical oncology* (June 2011). 1

[CTC*06] CARTER T. J., TANNER C., CRUM W. R., BEECHEY-NEWMAN N., HAWKES D. J.: A framework for image-guided breast surgery. In *MIAR'06* (2006), pp. 203–210. 2

[DGBW08] DICK C., GEORGII J., BURGKART R., WESTERMANN R.: Computational steering for patient-specific implant planning in orthopedics. In *Proceedings of Visual Computing for Biomedicine 2008* (2008), pp. 83–92. 2, 4

[DGW11] DICK C., GEORGII J., WESTERMANN R.: A real-time multigrid finite hexahedra method for elasticity simulation using CUDA. *Simulation Modelling Practice and Theory 19*, 2 (2011), 801–816. 2

[dPCH*08] DEL PALOMAR A. P., CALVO B., HERRERO J., LÓPEZ J., DOBLARÉ M.: A finite element model to accurately predict real deformations of the breast. *Medical engineering & physics 30*, 9 (2008), 1089–1097. 2

[GLDW10] GEORGII J., LAGLER D., DICK C., WESTERMANN R.: Interactive deformations with multigrid skeletal constraints. In *Proceedings of the 7th Workshop On Virtual Reality Interaction and Physical Simulation* (2010), pp. 39–47. 5

[GW08] GEORGII J., WESTERMANN R.: Corotated finite elements made fast and stable. In *Proceedings of the 5th Workshop On Virtual Reality Interaction and Physical Simulation* (2008), pp. 11–19. 4

[GW10] GEORGII J., WESTERMANN R.: A streaming approach for sparse matrix products and its application in Galerkin multigrid methods. *Electronic Transactions on Numerical Analysis 37* (2010), 263–275. 4

[HGSH11] HARZ M., GEORGII J., SCHILLING K. J., HAHN H. K.: Towards navigated breast surgery using efficient breast deformation simulation. In *Medical Image Computing and Computer-Assisted Intervention, Workshop on Breast Image Analysis* (September 2011), C. Tanner AND J. Schnabel AND N. Karssemeijer AND Mads Nielsen And M. Giger AND D. Hawkes, (Ed.). 2, 4

[HHM*11] HAN L., HIPWELL J., MERTZANIDOU T., CARTER T., MODAT M., OURSELIN S., HAWKES D.: A hybrid FEM-based method for aligning prone and supine images for image guided breast surgery. *ISBI 2011* (2011), 1239–1242. 2, 6

[MHH*12] MERTZANIDOU T., HIPWELL J. H., HAN L., TAYLOR Z., HUISMAN H., BICK U., KARSSEMEIJER N., HAWKES D. J.: Intensity-based mri to x-ray mammography registration with an integrated fast biomechanical transformation. In *IWDM 2012* (2012), Maidment A. D. A., Bakic P. R., Gavenonis S., (Eds.), vol. LNCS 7361, pp. 48–55. 5

[MSP10] MALLAPRAGADA V., SARKAR N., PODDER T. K.: Toward a Robot-Assisted Breast Intervention System. *Mechatronics, IEEE/ASME Transactions on PP*, 99 (2010), 1–10. 1

[RB86] RANKIN C., BROGAN F.: An element-independent corotational procedure for the treatment of large rotations. *ASME J. Pressure Vessel Tchn. 108* (1986), 165–174. 4

[RCB*07] RAJAGOPAL V., CHUNG J.-H., BULLIVANT D., NIELSEN P. M. F., NASH M. P.: Determining the finite elasticity reference state from a loaded configuration. *International Journal for Numerical Methods in Engineering 72*, 12 (2007), 1434–1451. 2, 9

[RNHN08] RAJAGOPAL V., NASH M. P., HIGHNAM R. P., NIELSEN P. M.: The Breast Biomechanics Reference State for Multi-modal Image Analysis. In *IWDM '08: Proceedings of the 9th international workshop on Digital Mammography* (2008), Springer-Verlag. 2

[RSM*06] RUITER N., STOTZKA R., MULLER T., GEMMEKE H., REICHENBACH J., KAISER W.: Model-based registration of X-ray mammograms and MR images of the female breast. *IEEE Transactions on Nuclear Science 53*, 1 (2006), 204–211. 3

[SGW07] SCHIWIETZ T., GEORGII J., WESTERMANN R.: Freeform image. In *Proceedings of Pacific Graphics* (2007). 4

[SKW10] SCHNEIDER J., KRAUS M., WESTERMANN R.: GPU-based euclidean distance transforms and their application to volume rendering. In *selected papers of VISIGRAPP 2009, Communications in Computer and Information Science (CCIS) 68* (2010), Springer-Verlag Berlin Heidelberg, pp. 215–228. 5

[SNT*98] SATO Y., NAKAMOTO M., TAMAKI Y., SASAMA T., SAKITA I., NAKAJIMA Y., MONDEN M., TAMURA S.: Image guidance of breast cancer surgery using 3-D ultrasound images and augmented reality visualization. *Medical Imaging, IEEE Transactions on 17*, 5 (1998), 681–693. 1

[TWG*11] TANNER C., WHITE M., GUARINO S., HALL-CRAGGS M. A., DOUEK M., HAWKES D. J.: Large breast compressions: observations and evaluation of simulations. *Medical physics 38*, 2 (Feb. 2011), 682–690. 2

[WFFH11] WANG L., FILIPPATOS K., FRIMAN O., HAHN H.: Fully automated segmentation of the pectoralis muscle boundary in breast MR images. In *SPIE Medical Imaging, Computer-Aided Diagnosis* (2011), vol. 7963. 3

[WGCB07] WHITELEY J. P., GAVAGHAN D. J., CHAPMAN S. J., BRADY J. M.: Non-linear modelling of breast tissue. *Mathematical Medicine and Biology 24*, 3 (Sept. 2007), 327–345. 2